



Cloud water adjustments to aerosol perturbations are buffered by solar heating in non-precipitating marine stratocumuli

Jianhao Zhang^{1,2}, Yao-Sheng Chen^{1,2}, Takanobu Yamaguchi^{1,2}, and Graham Feingold²

¹Cooperative Institute for Research in Environmental Sciences (CIRES), University of Colorado, Boulder, CO, USA

²Chemical Sciences Laboratory, National Oceanic and Atmospheric Administration (NOAA), Boulder, CO, USA

Correspondence: Jianhao Zhang (jianhao.zhang@noaa.gov)

Abstract. Marine low-level clouds are key to the Earth's energy budget due to their expansive coverage over global oceans and their high reflectance of incoming solar radiation. Their responses to anthropogenic aerosol perturbations remain the largest source of uncertainty in estimating the anthropogenic radiative forcing of climate. A major challenge is the quantification of the cloud water response to aerosol perturbations. In particular, the presence of feedbacks through microphysical, dynamical and thermodynamical pathways at various spatial and temporal scales could augment or weaken the response. Central to this problem is the temporal evolution in cloud adjustment, governed by entangled feedback mechanisms. We apply an innovative conditional Monte Carlo subsampling approach to a large ensemble of diurnal large-eddy simulation of non-precipitating marine stratocumulus to study the role of solar heating in governing the evolution in the relationship between droplet number and cloud water. We find a persistent negative trend in this relationship at night, confirming the role of microphysically enhanced cloud-top entrainment. After sunrise, the evolution in this relationship appears buffered and converges to ~ -0.2 in the late afternoon. This buffering effect is attributed to a strong dependence of cloud-layer shortwave absorption on cloud liquid water path. These diurnal cycle characteristics further demonstrate a tight connection between cloud brightening potential and the relationship between cloud water and droplet number at sunrise, which has implications for the impact of the timing of advertent aerosol perturbations.

1 Introduction

Marine stratocumulus (Sc) clouds, found ubiquitously over subtropical oceans, are key to the Earth's radiation budget (Wood, 2012). They cool the Earth effectively through reflecting a considerable amount of incoming solar radiation (Bender et al., 2011; Stephens et al., 2012). The radiative effect of marine stratocumulus is governed by its macrophysical properties, such as areal coverage and liquid water path (LWP), and microphysical properties, such as cloud droplet number concentration (N_d) or drop size. Increases in atmospheric aerosol particles lead to more, smaller cloud droplets (Twomey, 1974, 1977), modulate the rate of warm cloud processes, e.g., collision-coalescence and entrainment mixing, and subsequently cause adjustments in cloud macrophysical properties (e.g., Albrecht, 1989; Bretherton et al., 2007; Wang et al., 2003; Xue and Feingold, 2006). The radiative forcing attributed to cloud adjustments in response to anthropogenic aerosol increases is currently poorly constrained,



especially for marine boundary layer clouds, and remains the largest source of uncertainty in projections of the future climate
25 (Boucher et al., 2013; Forster et al., 2021; Bellouin et al., 2020).

A key, yet uncertain, component of these cloud adjustments is the response of cloud water to aerosol perturbations. Con-
straining it is particularly challenging because the impact of aerosol on cloud LWP is bidirectional and regime-dependent
(Chen et al., 2014; Gryspeerdt et al., 2019; Possner et al., 2020; Toll et al., 2019). For precipitating clouds, an increase in
aerosol tends to increase LWP through precipitation suppression (Albrecht, 1989), whereas for non-precipitating clouds, LWP
30 decreases through enhanced turbulent entrainment of dry, free-tropospheric (FT) air at cloud top, attributed to smaller droplets
(Bretherton et al., 2007; Wang et al., 2003). Thus, the frequency of occurrence of different cloud states governs the overall
response of cloud water to aerosol perturbations, which depends strongly on large-scale meteorological conditions (e.g., Zhang
et al., 2022; Zhou et al., 2021; Zhang and Feingold, 2023).

Making the quantification of LWP adjustment to aerosol perturbations even more challenging is the presence of feedbacks
35 among system-wide microphysical, dynamical and thermodynamical processes at different spatiotemporal scales, acting to
buffer the system's response to perturbations (Stevens and Feingold, 2009). Quantifying aerosol effects on LWP in such a
buffered system requires understanding not only of individual causal mechanisms but also their timescales (Glassmeier et al.,
2021; Fons et al., 2023; Gryspeerdt et al., 2022). Therefore, characterizing the temporal evolution of cloud adjustments is
central to this problem, as it provides a way to assess the relative importance of individual mechanisms. Based on an ensemble
40 of nocturnal large-eddy simulation (LES) of marine stratocumulus, Glassmeier et al. (2021) suggested that the estimated
cooling effect due to aerosol-cloud interactions derived from ship-track observations may be an overestimation if the temporal
evolution in cloud water adjustment is not taken into account. Using satellite observations, Gryspeerdt et al. (2021) showed that
the N_d -LWP relationship between ship-tracks and their surroundings is indeed time-dependent and sensitive to the cloud and
meteorological states under which the aerosol perturbation occurs. More generally, studies using geostationary satellites (e.g.,
45 Qiu et al., 2024; Christensen et al., 2023; Smalley et al., 2024) and polar-orbiting satellites (e.g., Diamond et al., 2020; Zhang
and Feingold, 2023) have indicated diurnal variation in cloud adjustments to aerosol perturbations, such that LWP adjustments
become more negative in the afternoon. Through extrapolating the Terra (late morning) and Aqua (early afternoon) difference,
Gryspeerdt et al. (2022) demonstrated the importance of controlling initial cloud states to account for feedbacks in the system,
and found a negative, but weaker, N_d -LWP relationship when feedbacks are accounted for.

50 When it comes to the attribution of the diurnal variation in cloud adjustment to aerosol perturbations, an often overlooked,
yet important, process is the shortwave (SW) absorption in the cloud layer. The balance between SW heating and longwave
(LW) cooling plays a crucial role in governing the daytime evolution of cloud water in marine stratocumulus (e.g., Sandu et al.,
2008; Chen et al., 2024). Since cloud SW absorption is a strong function of LWP and also dependent on N_d (Petters et al.,
2012), it can potentially act as an important feedback (or "buffering", in the case of a negative feedback) mechanism as cloud
55 water changes throughout the sunlit hours.

In this study, we aim to characterize the diurnal evolution in cloud water adjustments to aerosol perturbations, with a partic-
ular focus on understanding the importance of SW absorption in affecting this evolution. We have performed a large ensemble
of diurnal simulations of non-raining marine stratocumulus that represents conditions in the Northeastern Pacific region, using



an LES model that resolves aerosol-cloud interactions. By applying a novel subsampling approach (introduced in Sec. 2), we
60 find that cloud SW absorption acts to flatten the N_d -LWP relationship (indicated by regression slope) after sunrise, suggesting
a buffered evolution in cloud water response to aerosol perturbations (Sec. 3.1). Enlightened by these results, we further use
the subsampling approach to demonstrate a tight connection between the potential for cloud brightening and the cloud water to
droplet number relationship at sunrise (Sec. 3.2), with implications for the optimal timing of deliberate aerosol perturbations
in the context of Marine Cloud Brightening (MCB), one of the proposed climate intervention approaches (National Academies
65 of Sciences, Engineering, and Medicine (NASEM) report, 2021; Latham and Smith, 1990; Latham et al., 2012).

2 Methods and Data

While process-model-based perturbation experiments offer a great deal of understanding of the causal mechanisms driving
cloud adjustments to aerosol perturbations (e.g., Prabhakaran et al., 2023, 2024; Chun et al., 2023), these studies are typically
limited in their ability to represent the range of boundary layer conditions observed in nature. A new approach in the recent
70 decade suggests that one can infer process-level understanding from the systematic behavior of simulation ensemble(s) that
depict the evolution of cloud systems from a wide range of initial boundary layer conditions (e.g., Glassmeier et al., 2019, 2021;
Hoffmann et al., 2020, 2023), as a way to bridge “Newtonian” (bottom-up) and “Darwinian” (top-down) approaches (Feingold
et al., 2016; Mülmenstädt and Feingold, 2018). Following this methodology, we analyze a large ensemble of diurnal simulations
of marine stratocumulus with an innovative subsampling approach, in which the large ensemble is sub-grouped into smaller
75 ensembles as a means to investigate the impact of N_d on cloud water evolution and how it is mediated by SW heating.

2.1 Large-eddy simulation ensemble of marine stratocumulus

All simulations used in this study are carried out with the System for Atmospheric Modeling (SAM; Khairoutdinov and
Randal, 2003). The model domain size is set to $48 \times 48 \times 2.5$ km³ with a horizontal and vertical grid spacing of 200 m and 10 m,
respectively. This setup allows for development of mesoscale organizations (Kazil et al., 2017) while keeping computational
80 cost affordable for a large ensemble of simulations. All simulations are run for 24 h from 18:40 local time right after sunset
at a time step of 1 s. Cloud microphysical processes are simulated with a two-moment, bin-emulating bulk microphysical
scheme (Feingold et al., 1998) with prognostic total number concentration and total water content (Yamaguchi et al., 2019).
Aerosol number concentration (N_a) is prescribed to be initially uniform throughout the domain, and we assume a lognormal
aerosol size distribution (ammonium sulfate) with geometric-mean diameter of 0.2 μ m and geometric standard deviation of
85 1.5 μ m, following Feingold et al. (2016). Aerosol particles are lost to cloud and precipitation processing, such as collision-
coalescence, scavenging, and wet deposition, and we apply a constant surface flux of aerosol of 70 cm⁻² s⁻¹ (Yamaguchi et al.,
2017; Kazil et al., 2011) to mitigate depletion of aerosol. Radiative heating rates are calculated interactively every 10 s using
the Rapid Radiative Transfer Model (RRTMG; Clough et al., 2005) with extended thermodynamic profiles above the domain
top (2.5 km), following Yamaguchi et al. (2017). Surface sensible and latent heat fluxes are calculated interactively based
90 on Monin-Obukhov similarity and initialized with climatological mean surface winds. We prescribe a constant sea surface



temperature (SST) of 292.4 K, based on ERA5-derived climatology of large-scale meteorological conditions associated with the stratocumulus deck off the coast of California (Hersbach et al., 2020), and a fixed large-scale divergence of $3.75 \times 10^{-6} \text{ s}^{-1}$ (Ackerman et al., 2009) for all simulations. The reader is referred to Chen et al. (2024) for more technical details on the setup of the simulations.

95 Keeping the above model setup and large-scale forcings the same for all simulations, we vary the initial conditions for boundary layer (BL) thermodynamics in a six-parameter variable space to create ensemble members, using a maximin Latin-Hypercube sampling approach (Morris and Mitchell, 1995) to minimize correlations between parameters, as described in Feingold et al. (2016) and Glassmeier et al. (2019). The six parameters include: BL liquid water potential temperature ($284 \leq \theta_l \leq 294 \text{ K}$), BL total water mixing ratio ($6.5 \leq q_t \leq 10.5 \text{ g kg}^{-1}$), the jumps of temperature and humidity between BL and FT ($6 \leq \Delta\theta_l \leq 10 \text{ K}$ and $-10 \leq \Delta q_t \leq 0 \text{ g kg}^{-1}$), initial mixed-layer depth ($500 \leq h_{\text{mix}} \leq 1300 \text{ m}$), and aerosol number concentration ($30 \leq N_a \leq 500 \text{ mg}^{-1}$). Using the Latin-Hypercube sampling approach, we generate hundreds of initial thermodynamic profiles, from which we carry out simulations whenever a cloud layer is produced, and when the lifting condensation level is between 225 m and 1075 m and the FT θ_l and q_t profiles are within the ERA5 climatology of the Northeastern Pacific. This yields a total of 316 diurnal simulations. Since we focus on the non-precipitating marine stratocumulus system, we impose a threshold of 0.5 mm d^{-1} on cloud base rain rate to screen for non-raining simulations (Wood, 2012). We further exclude simulations that generate a surface fog, cloud tops higher than 2 km, and domain cloud fraction (f_c) less than 0.01 (full cloud dissipation) to ensure the robustness of our analysis when the subsampling is applied. Domain-mean 2-dimensional and 3-dimensional outputs are saved every 2 min and every hour, respectively. A total of 204 non-precipitating simulations are selected for analysis. We discard the first 4 h of all simulations as model spin-up and use a cloud optical depth (τ) threshold of one to identify clouds. A higher threshold of $\tau = 5$ was tested but did not change the conclusions qualitatively.

2.2 A conditional Monte Carlo sampling approach

Many recent studies (e.g., Gryspeerdt et al., 2016, 2019; Glassmeier et al., 2021; Zhang et al., 2022; Zhou et al., 2021; Smalley et al., 2024) have chosen to infer the impact of aerosol on cloud properties by examining the spatiotemporal correlation between cloud macrophysical properties and N_d , with N_d serving as an intermediate variable, in order to mitigate the influence of confounding factors on the causal relationship between aerosol and clouds and to avoid uncertainties in relating aerosol information, such as aerosol optical depth and aerosol index, to cloud condensation nuclei (CCN; Stier, 2016). Here, we adopt the same methodology and focus on the relationship between N_d and LWP, quantified as the slope of linear regressions (e.g., McComiskey and Feingold, 2012). Least-squares log regressions are used to alleviate the dependence of regression-slope on the absolute value of N_d (e.g., Feingold et al., 2003; Zhang et al., 2022).

120 Nevertheless, co-varying meteorological and aerosol conditions can still confound the N_d –LWP relationship in observations (e.g., Gryspeerdt et al., 2019) and in model simulations (e.g., Mülmenstädt et al., 2024). Therefore, we introduce a subsampling approach that can be conditioned on prescribed relationships among N_d , LWP, and initial boundary layer conditions, following the Monte Carlo methodology (Hammersley and Handscomb, 1964) with modifications to enable selection of specified conditions. We term this sub-sampling approach “conditional Monte Carlo (cMC).” The fundamental idea of employing the Monte



125 Carlo concept is to use repetitive, semi-random (i.e., conditional) samplings to capture systematic behaviors (deterministic in principle) of stochastically initialized realizations of marine Sc evolutions. The purpose of the cMC approach in this work is three-fold. First, it serves to help constrain the co-variation between N_d and meteorological conditions under which the simulations are initialized, which could confound the effect of N_d on LWP. Second, it serves as a means to free ourselves from dealing with an initially positive (after spin-up) N_d –LWP relationship imposed purely by the Latin-Hypercube sampling used
130 to construct the initial boundary layer conditions. Third, we use it to select N_d –LWP relationships and observe their temporal evolutions. In this work, we use statistical regression slopes to indicate the relationship (not necessarily causal) between two variables (e.g., N_d and LWP). The application of the cMC method alleviates the concern whether statistical slopes can indicate causal relationships, as we focus on the *evolution* rather than the absolute value of these slopes by selecting a range of slopes at sunrise.

135 The cMC approach is applied as follow. We first randomly draw 25 simulations from the 204 LES ensemble members (non-precipitating), using a random seed generator assuming a normal distribution. The “conditional” part of cMC is implemented such that a drawing is saved only when the following conditions are met: first, the co-variation between N_d and three boundary layer conditions (abbreviated as MET hereafter) at the beginning of the simulation (4 h) is smaller than user-imposed thresholds (i.e., minimizing the correlation between N_d and MET after spin-up). These three variables are cloud top height (z_{ct} ; a measure
140 of boundary layer depth), surface sensible heat flux (SHF), and 800 hPa relative humidity (RH_{800}), and the thresholds are: $-0.05 \leq d\ln(z_{ct})/d\ln(N_d) \leq 0.05$, $-0.5 \leq dSHF/d\ln(N_d) \leq 0.5$, and $-0.05 \leq d\ln(RH_{800})/d\ln(N_d) \leq 0.05$. Second, the N_d –LWP regression slope is close enough, within uncertainty ranges, to a user-prescribed value – essentially prescribing a cloud water to droplet number relationship for the randomly drawn 25 simulations. In our first investigation (Sec. 3.1), we prescribe 5 values for N_d –LWP slope ($d\ln(LWP)/d\ln(N_d)$) at sunrise: ± 0.4 (± 0.02), ± 0.2 (± 0.01), and 0 (± 0.005), to examine the
145 role of SW heating. In our second investigation (Sec. 3.2), we prescribe flat slopes for N_d –LWP and N_d – f_c , i.e., $-0.005 \leq d\ln(LWP)/d\ln(N_d) \leq 0.005$ and $-0.05 \leq df_c/d\ln(N_d) \leq 0.05$ to mimic the relationship between cloud micro- and macro-properties at the time of aerosol perturbation, representing a difference in the timescale between the “instantaneous” (order of minutes) microphysical response and the slower (order of hours) macrophysical adjustments.

Within each 25-member subgroup of simulations, we calculate the slope between N_d and LWP as $d\ln(LWP)/d\ln(N_d)$ at
150 each time step. We focus on the temporal *evolution* in $d\ln(LWP)/d\ln(N_d)$, in particular on the difference between nighttime and sunlit hours (Sec. 3.1) and the impact of N_d –LWP relationship at sunrise on time-integrated cloud radiative effect (Sec. 3.2), rather than the absolute value of $d\ln(LWP)/d\ln(N_d)$, which we prescribe when subsampling. The drawing is repeated with the same pre-conditions but different random number seeds to produce 50 25-member subgroups, and the mean evolution (averaged over 50 repetitions) is shown in the results. We also tested other configurations of the cMC setup, varying the
155 number of members within each draw, number of draws, and the user-imposed thresholds. Different configurations yield the same conclusions, qualitatively, and the choice of the current configuration is based on computing efficiency.



3 Results

3.1 The role of SW absorption in affecting diurnal evolution in N_d -LWP relationship

3.1.1 A buffered evolution during the daytime

160 Besides the variations in N_d being a fundamental perturbation to the Sc system, the impact of solar heating on cloud water evolution starting from sunrise is another important perturbation to the system. During daytime, the sensitivity of radiation to cloud macro- and micro-physical properties is critical to the evolution in the N_d -LWP slope. In particular, the dependence of cloud-layer LW cooling on LWP and N_d is only apparent in thin clouds and saturates at around 20 to 30 g m⁻², whereas SW heating increases continuously as LWP and N_d increase, more pronouncedly with LWP (Petters et al., 2012). The different

165 sensitivities of solar heating to LWP and N_d , which vary among LES ensemble members, are hypothesized to affect the daytime evolution in the N_d -LWP slope. In order to examine the effects of solar heating on the cloud water to droplet number relationship, we subsample using the cMC approach five conditions where subsampled simulations possess prescribed N_d -LWP slopes at sunrise, ranging from -0.4 to 0.4 with an increment of 0.2 (Sec. 2.2). The diurnal evolution in the N_d -LWP slope of the five subgroups is shown in Figure 1, with the red curve indicating the most positive (0.4) N_d -LWP slope at sunrise

170 and the blue curve representing the most negative (-0.4) one. A persistent feature of the N_d -LWP slopes becoming more negative with time is observed at night, consistent with the findings in Glassmeier et al. (2021), regardless of the prescribed slopes at sunrise. This is attributed to the sensitivity of turbulent entrainment at cloud top to drop size, such that smaller drops (higher N_d) promote stronger entrainment. A sensitivity of the entrainment mechanism to LWP is also evident in the nighttime evolution where the decrease in the N_d -LWP slope for the group that starts with an initially positive N_d -LWP slope (higher

175 N_d associated with higher LWP) is faster (from 1 to 0.4, red), compared to that in the group starting with a negative slope (from -0.1 to -0.4, blue; Fig. 1).

Interesting evolution in the N_d -LWP slope appears a couple of hours after sunrise where groups starting from very different N_d -LWP slopes at sunrise begin to converge (Fig. 1). The group convergence shares features typical to buffered evolution, such that the groups starting with a negative slope become less negative, whereas the groups starting with a positive slope become

180 less positive over time. We will show that the cause of such a buffered evolution during the day is the primary dependence of SW heating on cloud LWP, such that thicker clouds (higher LWP) experience stronger cloud thinning with stronger SW absorption whereas thinner clouds thin more slowly with weaker SW absorption, leading to flattening of all N_d -LWP slopes, regardless of their values at sunrise. For this task, we will need to quantify the rate of change in LWP attributed to radiative processes. Hence, we performed a budget analysis of the LWP tendency, following Chen et al. (2024), to further illustrate this

185 attribution in the following.

3.1.2 The sensitivity of LWP tendency to N_d

The impact of N_d perturbations on cloud LWP is through affecting the rates of processes that govern the budget of cloud water. Here, we focus on two terms in this budget that are known to be sensitive to cloud water and droplet number, namely



190 entrainment and radiation processes, derived as below, following Chen et al. (2024). First, the total rate of change of cloud LWP is written as

$$\mathcal{L}' = \Gamma_1 \langle \rho_0 \rangle (z_{\text{inv}} - z_{\text{cb}}) \left[z'_{\text{inv}} - \left(\frac{dz_{\text{cb}}}{d\langle q_t \rangle} \langle q_t \rangle' + \frac{dz_{\text{cb}}}{d\langle \theta_1 \rangle} \langle \theta_1 \rangle' \right) \right], \quad (1)$$

where \mathcal{L} denotes LWP, ' denotes time-derivatives, z_{cb} is the mean cloud base height, z_{inv} is the mean inversion base height, and Γ_1 is the liquid water adiabatic lapse rate. We then decompose $\langle q_t \rangle'$ and $\langle \theta_1 \rangle'$ into individual budget terms grouped by processes ($\langle \phi \rangle'_{\text{process}}$), e.g., radiation (RAD) and entrainment (ENT). $\langle \phi \rangle$ is the volume-mean of a scalar quantity that represents either q_t or θ_1 in our case. In particular, $\langle \phi \rangle'_{\text{RAD}}$ is straightforwardly calculated from the 3-dimensional, modeled radiative heating rates, and $\langle \phi \rangle'_{\text{ENT}}$ is approximated by the difference between the total tendency of $\langle \phi \rangle$ in the boundary layer (BL) and the sum of contributions from all processes other than ENT, which can be directly estimated from the modeled fields. The reader is referred to Chen et al. (2024) for more details on the derivation and justification of assumptions for the LWP tendency budget analysis.

200 First, we show the mean evolution in LWP tendencies attributed to entrainment, radiation and their net effect (Fig. 2a). $\mathcal{L}'_{\text{RAD}}$ remains constant throughout the night, consistent with the saturation of the dependence of LW cooling on LWP when clouds are still relatively thin. $\mathcal{L}'_{\text{ENT}}$ strengthens weakly as cloud thickens during the night. After sunrise, SW heating offsets LW cooling and weakens the entrainment mixing at cloud tops. During cloud recovery in the late afternoon, the impacts of radiation and entrainment on LWP tendency balance each other. We caution that during the late afternoon the residual of the budget analysis increases, and for this reason, we limit our interpretation of the LWP budget evolution to the hours before 15 local time.

Next, we investigate the sensitivity of LWP tendency to N_d , (i.e., $\mathcal{L}''_{\text{ENT}}$, $\mathcal{L}''_{\text{RAD}}$, and $\mathcal{L}''_{\text{ENT+RAD}}$ where the second ' indicates derivatives with respect to $\ln(N_d)$; Fig. 2b-d), focusing on their role in governing the evolution in $d\ln(\text{LWP})/d\ln(N_d)$, as seen in Figure 1. Different colors in Figure 2 (b-d) represent exactly the same subgroups conditioned on prescribed values of $d\ln(\text{LWP})/d\ln(N_d)$ at sunrise, i.e., from -0.4 to 0.4. An important note to keep in mind is that these sensitivities to N_d inherently include sensitivities to LWP, because we prescribed the N_d -LWP slope in these subgroups, such that high N_d is associated with high LWP when $d\ln(\text{LWP})/d\ln(N_d)$ is positive (e.g., the red line), and high N_d is associated with low LWP for a negative $d\ln(\text{LWP})/d\ln(N_d)$ (e.g., the blue line).

215 During the night, the net effect of entrainment and radiation on the LWP tendency (Fig. 2c) nicely explains the persistent decreasing trend in $d\ln(\text{LWP})/d\ln(N_d)$ (Fig. 1). The negative values in $\mathcal{L}''_{\text{ENT+RAD}}$ (regardless of the prescribed $d\ln(\text{LWP})/d\ln(N_d)$ values) suggest that clouds with higher N_d experience stronger LWP loss, resulting in the N_d -LWP slope becoming more negative with time. This effect is primarily driven by the $\mathcal{L}''_{\text{ENT}}$ term (Fig. 2b), consistent with the entrainment-enhancement mechanism due to more smaller droplets (Wang et al., 2003). When cloud water and droplet number are positively correlated (the red line), the sensitivity of the LWP tendency to N_d ($\mathcal{L}''_{\text{ENT+RAD}}$) is found to be the strongest (Fig. 2c), confirming the fastest decrease of $d\ln(\text{LWP})/d\ln(N_d)$ in that subgroup (Fig. 1), as both higher N_d and higher LWP induce stronger entrainment.

220 After sunrise, a feature essential to explaining the buffered evolution in $d\ln(\text{LWP})/d\ln(N_d)$ emerges, that is $\mathcal{L}'_{\text{ENT+RAD}}$ in subgroups with a negative $d\ln(\text{LWP})/d\ln(N_d)$ at sunrise (i.e., blue and cyan) become positively correlated with N_d (Fig.



2c), indicating a reverse of the persistent nighttime negative trend in $d\ln(\text{LWP})/d\ln(N_d)$, which leads to the flattening of the negative N_d -LWP slopes (Fig. 1). Radiation, especially SW heating, plays a critical role here by dominating the contribution to the stratification feature observed in $\mathcal{L}''_{\text{ENT+RAD}}$ between 10 and 11 local time (Fig. 2d). This would not be the case if $\mathcal{L}''_{\text{RAD}}$ were to follow its trend during the nighttime as if there were no solar radiation. The dependence of solar heating on N_d and especially cloud water is key. Unlike LW cooling, whose dependence on LWP saturates when clouds are still relatively thin, the dependence of SW heating on LWP persists in thicker clouds (Petters et al., 2012), such that thick clouds absorb more SW than thin clouds – a positive slope between SW heating and LWP. This leads to a negative slope between $\mathcal{L}'_{\text{RAD}}$ and LWP, given that LW cooling still dominates the contribution of radiative processes to the LWP tendency in the daytime, i.e., $\mathcal{L}'_{\text{RAD}}$ is positive in the mean (Fig. 2a, red line). In other words, higher LWP induces more SW heating, or stronger offsetting of the LW cooling, leading to a weaker LWP tendency due to radiation. Effectively, the inclusion of SW radiation reverses the slope between $\mathcal{L}'_{\text{RAD}}$ and N_d , regardless of the prescribed N_d -LWP slope (Fig. 2d). When a positive N_d -LWP slope is imposed at sunrise, this translates into a negative slope between $\mathcal{L}'_{\text{RAD}}$ and N_d (red line in Fig. 2d), whereas when N_d and LWP are negatively correlated, $\mathcal{L}''_{\text{RAD}}$ is positive (Fig. 2d, blue line). The fact that the dependence of $\mathcal{L}'_{\text{RAD}}$ on LWP is able to explain the observed evolution in $\mathcal{L}''_{\text{RAD}}$ suggests that the effect of N_d on the LWP tendency driven by radiative processes is secondary to the impact of LWP. In other words, if the counter hypothesis is true, that is the N_d -impact is not secondary to the LWP-impact (or comparable to the LWP-impact), then $\mathcal{L}''_{\text{RAD}}$ should be skewed towards negative values after sunrise, as the LWP-impact and the N_d -impact offset (complement) each other in the case of a negative (positive) N_d -LWP slope. Therefore, we conclude that the buffered evolution observed in $d\ln(\text{LWP})/d\ln(N_d)$ after sunrise (Fig. 1) can be attributed to the primary dependence of SW heating on cloud water.

To summarize, we have identified two features associated with the diurnal evolution of the cloud water to droplet number relationship for non-precipitating Sc, that are 1) the N_d -LWP slope becomes more negative with time at night, and 2) the N_d -LWP slope flattens (is buffered) after sunrise due to the strong dependence of SW heating on cloud LWP than on N_d . A schematic summarizing the latter point is shown in Figure 3 where thicker clouds (higher LWP) experience stronger cloud thinning, resulting in flattening of the N_d -LWP slope. Keeping these two features in mind, we next explore the dependence of the cloud radiative effect, in the form of daytime-integrated SW reflection, on the relationship between cloud water and droplet number at sunrise.

3.2 The role of N_d -LWP relationship at sunrise in governing the daytime cloud radiative effect

When we assess the radiative effect at the top-of-the-atmosphere (TOA) due to aerosol-cloud-interactions (ACI), the reflectance from the entire Sc scene matters. In other words, the all-sky SW albedo of the cloud field is governed by its areal coverage (f_c) and the optical thickness of the cloud, which is a function of its LWP and N_d (i.e., $\tau \propto \text{LWP}^{\frac{5}{6}} N_d^{\frac{1}{3}}$, based on the adiabatic assumption; Boers and Mitchell, 1994). Using a 2-stream approximation to relate changes in cloud albedo (A_c) to changes in τ (Platnick and Twomey, 1994), one can show that the the sensitivity of A_c to N_d perturbations (S) follows the form of

$$S = \frac{dA_c}{d\ln(N_d)} = \frac{A_c(1 - A_c)}{3} \left(1 + \frac{5}{2} \frac{d\ln(\text{LWP})}{d\ln(N_d)} \right). \quad (2)$$



Clearly, one sees that the subject of this study – the cloud water to droplet number relationship ($d\ln(\text{LWP})/d\ln(N_d)$) – is central to this equation, in the sense that close to -0.4 it could determine the sign of S , i.e., cloud brightening or darkening. As demonstrated in the previous section, diurnal evolution in $d\ln(\text{LWP})/d\ln(N_d)$ is sensitive to its value at sunrise. This motivates us to further investigate the effect of the N_d -LWP slope at sunrise on the daytime cloud radiative effect due to N_d perturbations. Given the persistent decreasing trend in $d\ln(\text{LWP})/d\ln(N_d)$ during the night (Fig. 1), one can relate the sunrise value of $d\ln(\text{LWP})/d\ln(N_d)$ to how long it has been since the perturbation in N_d is introduced. This is because at the time when an aerosol perturbation is applied to a Sc system, we know that N_d responds to the addition of aerosol much more quickly than the amount of cloud water and its horizontal extent (i.e., cloud fraction) adjust to the new microphysical state of the cloud, resulting in a flat slope between cloud micro- and macro- physical properties. As a result, the earlier the N_d perturbation is applied the more negative $d\ln(\text{LWP})/d\ln(N_d)$ will be at sunrise, as $d\ln(\text{LWP})/d\ln(N_d)$ persistently decreases during the night.

We use the cMC method to subsample conditions where a 25-member subset of the LES ensemble has near-zero (in a statistical sense) N_d -LWP and N_d - f_c slopes, in addition to the constraint on N_d -MET covariations (see Sec. 2.2 for the threshold values used to impose these constraints). We vary the time at which we impose these near-zero slopes, ranging from 22:40 to 05:40 (~sunrise) local time with an increment of 1 h, yielding eight subsampled groups whose diurnal evolutions in the slope between cloud properties (LWP, f_c , A_c , and SW reflection) and N_d are further examined. Our subsampling strategy also enables implications for real-world applications where intentional aerosol perturbations, such as MCB, are considered.

A subtlety here is the interpretation of N_d - f_c relationships (quantified as $df_c/d\ln(N_d)$), as the diurnal evolutions in f_c between open-cell (non-raining) and closed-cell are distinct from each other (e.g., Fig. 4). Besides, open-cell Sc clouds can have quite different cloud-top entrainment characteristics, compared to closed-cell clouds (e.g., Abel et al., 2020). For these reasons, we further classify the 204 non-precipitating cases into 1) overcast closed-cell Sc and 2) non-precipitating open-cell Sc, based on f_c values at night. A total of 114 simulations where f_c remains 1 from ~22:40 (local time; after spin-up) to sunrise are classified into 1) and the rest (90 runs) are classified into 2). Figure 4 shows example snapshots of the cloud field at midnight and the mean cloud behaviors of these two classes. For overcast closed-cell Sc, clouds thin first while maintaining the overcast state before they start to breakup at $\sim 100 \text{ g m}^{-2}$ (Fig. 4 a). For non-precipitating open-cell Sc, clouds thicken and widen at the same time before sunrise and, in a similar manner, they thin and shrink after sunrise, creating a loop-like diurnal cycle in the LWP- f_c variable space (Fig. 4 b). Both classes of clouds begin to recover LWP and f_c after noon, except that the non-precipitating open-cell class recovers f_c faster.

3.2.1 Overcast closed-cell Sc

Figure 5 (a-d) shows the evolution of slopes between N_d and cloud properties, including LWP, f_c , cloud albedo (A_c), and upwelling SW radiation at TOA (SW_{up} ; a measure of reflected SW radiation by the entire cloud scene) for the eight cMC-subsampled groups (separated by colors). The N_d -LWP slope in all subgroups trends negatively with time during the night, and its evolution appears buffered after sunrise (Fig. 5a), consistent with the results shown in Sec. 3.1 (Fig. 1). The N_d - A_c slope is positive despite the negative N_d -LWP slope (Fig. 5c), in agreement with the critical N_d -LWP slope of -0.4 for the



290 LWP adjustment to overcome the Twomey effect (Eqn. 2). The evolution in the N_d - A_c slope closely tracks that in the N_d -LWP slope, suggesting a strong control of $d\ln(\text{LWP})/d\ln(N_d)$ over S . The clouds remain overcast throughout the night until late morning, when the thinnest clouds breakup earliest, resulting in a slight negative N_d - f_c slope, owing to the negative slope between N_d and LWP at sunrise, but only when $d\ln(\text{LWP})/d\ln(N_d)$ is strongly negative (e.g., blue line in Fig. 5). This is also evident in the relationships between N_d and the cloud breakup time ($d(\text{time}_{f_c < 0.95})/d\ln(N_d)$), where only the two groups
295 with the earliest perturbation time (thereby more negative $d\ln(\text{LWP})/d\ln(N_d)$ at sunrise) do not show a delayed breakup (Fig. 6, black) under high N_d conditions. After noon, the N_d - f_c slope becomes positive for all groups (Fig. 5b), attributed to a generally delayed diurnal cycle in both LWP and f_c (Fig. 6), meaning cloud thinning and breakup occur later in high N_d clouds due to weaker LWP and f_c tendencies when N_d and LWP are negatively correlated at sunrise (Fig. 5a and S1).

When we combine the effects of Twomey, LWP and f_c adjustments, it comes at no surprise that higher N_d leads to more reflected SW at TOA throughout the day (Fig. 5d), given that the negative $d\ln(\text{LWP})/d\ln(N_d)$ is not strong enough to overcome the Twomey effect (Fig. 5c) and that $df_c/d\ln(N_d)$ is mostly positive. Clearly, SW_{up} has the strongest sensitivity to N_d perturbations in the group with the latest “aerosol perturbation” (at sunrise; red line in Fig. 5d), which produces the greatest increase in the temporally integrated SW_{up} per unit increase in $\ln(N_d)$ (Fig. 5, filled squares). A critical difference between these groups is the N_d -LWP relationship at sunrise, which is important for daytime cloud tendencies and strongly tied to the
305 time of “aerosol perturbation” in this setup.

3.2.2 Non-precipitating open-cell Sc

Similar evolutions in N_d -LWP and N_d - A_c slopes are found in non-precipitating open-cell Sc (Fig. 7a and c). In contrast to the evolution in N_d - f_c slope for the overcast closed-cell Sc where different groups track each other quite closely throughout the day, the N_d - f_c slope after sunrise stratifies by both the N_d -LWP and the N_d - f_c slopes at sunrise in the non-precipitating
310 open-cell Sc (Fig. 7b). This is consistent with the characteristic diurnal cycle of LWP and f_c (Fig. 4b) such that they increase (or decrease) coherently with time, leading to a similarly buffered evolution in $df_c/d\ln(N_d)$ (Fig. 7b). Worth noting is that the buffering effect drives a sign-change in $df_c/d\ln(N_d)$ after noon for the groups with the latest “aerosol perturbation” (orange and red lines). A comparison between the earliest and the latest (at sunrise) “aerosol perturbation” groups (Fig. 8) reveals that for groups starting with already pronounced negative N_d -LWP and N_d - f_c slopes at sunrise (Fig. 8a), the effect of increasing
315 N_d is to shift the diurnal cycle towards lower LWP and lower f_c in general. However, for groups where LWP and f_c remain similar between high- and low- N_d clouds at sunrise (Fig. 8b), the addition of smaller cloud droplets reduces LWP gradually, a process that can be attributed to the enhanced cloud-top entrainment, while similar f_c is maintained. For both cases, cloud recovery is noted to be slightly hastened under high- N_d conditions (Fig. S2), which is likely facilitated by weaker SW heating due to reduced LWP. In the case of sunrise “perturbation” where f_c is only subtly adjusted, hastened f_c recovery leads to a
320 positive $df_c/d\ln(N_d)$ in the afternoon (Fig. 7b and 8).

This stratification in N_d - f_c slopes complements the radiative impact due to N_d -LWP stratification alone (Fig. 7a), leading to an even more pronounced stratification in $d\text{SW}_{\text{up}}/d\ln(N_d)$ evolution. As a result, the dependence of $d(\int \text{SW}_{\text{up}} dt)/d\ln(N_d)$ on “aerosol perturbation” time is more pronounced than that in the overcast closed-cell Sc (Fig. 7d, filled squares).



4 Discussion

325 Despite the wide usage of the statistical regression method to derive aerosol-cloud relationships from which process under-
standing is inferred, the extent to which these statistical relationships equate to a causal response, thereby representing cloud
adjustments has been a nagging concern of studies of this kind. More recently, there is evidence showing that the negative
branch of the observed inverted-V shape in the N_d -LWP relationship (e.g., Gryspeerdt et al., 2019) overestimates the true
causal effect of N_d on LWP (e.g., Arola et al., 2022; Fons et al., 2023). Using general circulation models (GCMs), Mülmen-
330 städt et al. (2024) demonstrate the possibility that the sign of the cloud adjustment inferred from the N_d -LWP relationship
derived from internal variabilities can even be misleading, which they attribute to the confounding effect of the covariation
between N_d and meteorological conditions.

We wish to note that the way we investigate the relationship between cloud water and droplet number, i.e., by subsampling
conditions where a subsample of the large simulation ensemble has a predetermined N_d -LWP relationship and by focusing
335 on its *evolution* rather than its absolute value, alleviates reliance on the interpretation of the N_d -LWP relationships as causal
relationships. In other words, the SW heating driven feedback (or buffering) mechanism we have uncovered in this work is
a genuine feature of the Sc system and does not depend on the actual (prescribed) value of $d\ln(\text{LWP})/d\ln(N_d)$ in the cMC
experiments or in the real world. From this perspective, we discuss the role that these results, in particular this feedback mech-
anism, play in the aerosol-cloud-interactions that we observe in nature, where the N_d -LWP relationship is not predetermined
340 and often confounded by other cloud controlling factors. In fact, a number of satellite-based studies have suggested that this
relationship in nature is strongly dependent on cloud regime, boundary layer characteristics, and the spatial scale of one's
investigation (e.g., Gryspeerdt et al., 2019; Possner et al., 2020; Toll et al., 2019; Zhou and Feingold, 2023). The essence of
this radiation-buffering is the dependence of LWP tendency attributed to radiation processes (SW absorption in particular) on
cloud LWP, meaning thicker clouds thin faster and thinner clouds thin more slowly (Fig. 3), flattening whatever slope N_d and
345 LWP may have had before sunrise, depending on the large-scale meteorological conditions the clouds have experienced, no
matter whether the N_d -LWP relationship is causal or not.

Moreover, one of the strengths of this novel subsampling approach is by design, to minimize the confounding effects from
the initial boundary layer conditions in this large ensemble of simulations and to address some of the aforementioned concerns.
Therefore, although our emphasis is not on quantifying actual cloud adjustments, we aim to advance our understanding of
350 the temporal evolution in adjustments. Consider the Marine Cloud Brightening (MCB) idea, one of the proposed climate
intervention approaches, as an example. When we think about how we might maximize the total amount of sunlight reflected
over a day if we were to seed non-precipitating Sc clouds to increase their reflectivity of solar radiation, we want neither a
negative LWP adjustment to start with nor do we want to seed after the sun is up. Given the persistent negative trend in the
nighttime evolution of $d\ln(\text{LWP})/d\ln(N_d)$ (Fig. 1 and Sec. 3.1), it is logical to propose that seeding at sunrise would be the
355 most effective brightening strategy, which our results in Sec. 3.2 have validated. This is attributed to the critical role of sunrise
values of cloud water, N_d , and their correlation in governing the daytime evolution of cloud fraction and LWP.



There are, of course, caveats to this implication. For one, we focus only on non-precipitating Sc systems, whereas studies have shown that suppressing or even stopping precipitation in Sc systems can potentially generate larger radiative impacts, compared to brightening the non-precipitating systems (e.g., Wang and Feingold, 2009; Prabhakaran et al., 2023, 2024; Chun et al., 2023). Moreover, given the typical lifetime of aerosol in the marine boundary layer (a few days; Wood, 2012, 2021), our integration over one diurnal cycle may seem short in terms of representing the full extent of the radiative impact due to seeding. Extending the analysis to three diurnal cycles results in similar conclusions on the persistent nighttime negative trend in N_d -LWP slope and the daytime buffering due to SW absorption, which essentially makes the N_d -LWP slope oscillate between -0.1 and -0.4 after convergence in the first afternoon (Fig. S3). That said, these non-precipitating Sc clouds tend to be advected by the prevailing winds in the region and experience pronounced large-scale forcing changes, e.g., warming SST and deepening marine boundary layer, which lead to transition into a more cumulus regime, during the course of 3 to 5 days over subtropical ocean basins (Bretherton and Wyant, 1997; Yamaguchi et al., 2017). Studies deploying large ensemble of multi-day Lagrangian simulations are warranted to further address this issue. While the implications of this particular exemplary application (i.e., MCB) is limited, the great potential of applying this cMC approach to simulation ensembles is demonstrated.

370 5 Conclusions

A novel conditional Monte Carlo (cMC) subsampling approach is applied to a large ensemble of diurnal LES simulation, in order to explore the role of solar heating in affecting the temporal evolution and timescale of cloud water adjustment to aerosol perturbations in non-precipitating marine stratocumulus. We find evidence supporting an important negative feedback (or buffering) mechanism in the daytime evolution of the N_d -LWP relationship such that a persistent decreasing trend at night is buffered (N_d -LWP slope becomes flattened) after sunrise, regardless of the actual value of $d\ln(\text{LWP})/d\ln(N_d)$. Using a budget analysis of the LWP tendency, we separate and quantify the contributions from individual processes to this tendency, including entrainment and radiation. This enables us to attribute this buffering effect to the primary dependence of SW heating on LWP. This result emphasizes the dominant role of cloud LWP in governing daytime cloud tendencies, especially those related to SW absorption. The impacts of N_d perturbations appear to be only secondary.

380 This SW-LWP buffering has important implications for the temporal evolution in cloud adjustments to aerosol perturbations and the timescale of adjustments. Among various feedback mechanisms through microphysical processes, such as evaporation and sedimentation, surface fluxes, and/or large-scale circulation adjustments (e.g., Wang et al., 2003; Bretherton et al., 2007; Chun et al., 2023; Dagan et al., 2023), the role of SW heating has received the least attention. The implications for aerosol-cloud radiative forcing of climate are yet to be fully evaluated.

385 The methodology applied to the large simulation ensemble (i.e., subsampling) differs from previous studies in which the whole ensemble is used at once to map emergent properties, such as the cloud radiative effect (Glassmeier et al., 2019) and their flow field from a wide range of initial conditions (e.g., Glassmeier et al., 2021; Hoffmann et al., 2020). This work demonstrates the substantial potential in the application of this cMC approach. It can enhance the usefulness of any large-



ensemble of simulations by generating numerous sub-ensembles, whose potential in scientific applications is well beyond that
390 of the original ensemble, without the need to increase the size of the original ensemble.

The cMC subsampling approach presents a new pathway to explore systematic behaviors in cloud evolution from a large
number of simulated realizations or observations while avoiding spurious covariations among cloud controlling factors that are
either related to the seemingly random initializations or meteorological confounding factors. This alleviates the need to assume
that spatiotemporal correlations can be used to infer causal relationships. Moreover, it enables one to select conditions where
395 hypothesis-driven constraints can be prescribed and tested.

The SW-LWP buffering mechanism and its important role in governing the diurnal evolution in cloud water response to
droplet number perturbations, also has implications for the assessment of the viability of MCB. The robust decreasing trend in
the N_d -LWP relationship at night motivates an MCB-oriented thinking on how one might maximize the sunlight reflected by a
cloud scene. Using the cMC subsampling approach as a way to mimic the timing of the aerosol perturbation, we make the case
400 that seeding at sunrise presents the highest potential for brightening. This statement is by no means an endorsement of MCB
as a viable climate intervention method. Much more solid research is needed at this stage to determine the viability of MCB
and to quantify the potential risks associated with it (Feingold et al., 2024).

Data availability. The System for Atmospheric Modeling (SAM) code is graciously provided by Marat Khairoutdinov, which is publicly
available at the Harvard repository (<https://wiki.harvard.edu/confluence/display/climatemodeling/SAM/>). Input files for reproducing the sim-
405 ulation data are available from the NOAA Chemical Sciences Laboratory's Clouds, Aerosol, & Climate program at https://csl.noaa.gov/groups/csl9/datasets/data/cloud_phys/2024-Zhang-et-al/.

Author contributions. JZ carried out the data analysis and wrote the manuscript with input from all authors. YSC and TY ran the simulation
ensemble. All authors contributed to the design of the study and the interpretation of the results.

Competing interests. At least one of the (co-)authors is a member of the editorial board of Atmospheric Chemistry and Physics. Other than
410 this, the authors declare that they have no conflict of interests.

Acknowledgements. We thank Franziska Glassmeier and Fabian Hoffmann for insightful comments and discussion. We thank [] and [] for
their insights and suggestions for improving our manuscript. We thank the NOAA Earth's Radiation Budget (ERB) for supporting this
research.

<https://doi.org/10.5194/egusphere-2024-1021>

Preprint. Discussion started: 16 April 2024

© Author(s) 2024. CC BY 4.0 License.



Financial support. This research has been supported in part by the U.S. Department of Energy, Office of Science, Atmospheric System
415 Research Program Interagency Award 89243023SSC000114, the U.S. Department of Commerce, Earth's Radiation Budget grant, NOAA
CPO Climate & CI #03-01-07-001, and the NOAA Cooperative Agreement with CIRES, NA22OAR4320151.



References

- Abel, S. J., Barrett, P. A., Zuidema, P., Zhang, J., Christensen, M., Peers, F., Taylor, J. W., Crawford, I., Bower, K. N., and Flynn, M.: Open cells exhibit weaker entrainment of free-tropospheric biomass burning aerosol into the south-east Atlantic boundary layer, *Atmos. Chem. Phys.*, 20, 4059–4084, <https://doi.org/10.5194/acp-20-4059-2020>, 2020.
- Ackerman, A. S., vanZanten, M. C., Stevens, B., Savic-Jovicic, V., Bretherton, C. S., Chlond, A., Golaz, J.-C., Jiang, H., Khairoutdinov, M., Krueger, S. K., Lewellen, D. C., Lock, A., Moeng, C.-H., Nakamura, K., Petters, M. D., Snider, J. R., Weinbrecht, S., and Zulauf, M.: Large-Eddy Simulations of a Drizzling, Stratocumulus-Topped Marine Boundary Layer, *Mon. Wea. Rev.*, 137, 1083–1110, <https://doi.org/10.1175/2008MWR2582.1>, 2009.
- Albrecht, B. A.: Aerosols, Cloud Microphysics, and Fractional Cloudiness, *Science*, 245, 1227–1230, <https://doi.org/10.1126/science.245.4923.1227>, 1989.
- Arola, A., Lipponen, A., Kolmonen, P., Virtanen, T. H., Bellouin, N., Grosvenor, D. P., Gryspeerdt, E., Quaas, J., and Kokkola, H.: Aerosol effects on clouds are concealed by natural cloud heterogeneity and satellite retrieval errors, *Nat. Commun.*, 13, <https://doi.org/10.1038/s41467-022-34948-5>, 2022.
- Bellouin, N., Quaas, J., Gryspeerdt, E., Kinne, S., Stier, P., Watson-Parris, D., Boucher, O., Carslaw, K., Christensen, M., Daniau, A.-L., Dufresne, J.-L., Feingold, G., Fiedler, S., Forster, P., Gettelman, A., Haywood, J., Lohmann, U., Malavelle, F., Mauritson, T., and Stevens, B.: Bounding global aerosol radiative forcing of climate change, *Rev. of Geophys.*, 58, e2019RG000660, <https://doi.org/10.1029/2019RG000660>, 2020.
- Bender, F. A.-M., Charlson, R. J., Ekman, A. M. L., and Leahy, L. V.: Quantification of Monthly Mean Regional Scale Albedo of Marine Stratiform Clouds in Satellite Observations and GCMs, *J. Appl. Meteor. Climatol.*, 50, 2139–2148, <https://doi.org/10.1175/JAMC-D-11-049.1>, 2011.
- Boers, R. and Mitchell, R. M.: Absorption feedback in stratocumulus clouds Influence on cloud top albedo, *Tellus A*, 46, 229–241, <https://doi.org/https://doi.org/10.1034/j.1600-0870.1994.00001.x>, 1994.
- Boucher, O., Randall, D., Artaxo, P., Bretherton, C., Feingold, G., Forster, P., Kerminen, V.-M., Kondo, Y., Liao, H., Lohmann, U., Rasch, P., Satheesh, S., Sherwood, S., Stevens, B., and Zhang, X.: Clouds and Aerosols, in: *Climate Change 2013: The Physical Science Basis. Contribution of Working Group I to the Fifth Assessment Report of the Intergovernmental Panel on Climate Change*, edited by Stocker, T., Qin, D., Plattner, G.-K., Tignor, M., Allen, S., Boschung, J., Nauels, A., Xia, Y., Bex, V., and Midgley, P., pp. 571–658, Cambridge University Press, Cambridge, United Kingdom and New York, NY, USA, 2013.
- Bretherton, C. S. and Wyant, M. C.: Moisture Transport, Lower-Tropospheric Stability, and Decoupling of Cloud-Topped Boundary Layers, *J. Atmos. Sci.*, 54, 148–167, [https://doi.org/10.1175/1520-0469\(1997\)054<0148:MTL TSA>2.0.CO;2](https://doi.org/10.1175/1520-0469(1997)054<0148:MTL TSA>2.0.CO;2), 1997.
- Bretherton, C. S., Blossey, P. N., and Uchida, J.: Cloud droplet sedimentation, entrainment efficiency, and subtropical stratocumulus albedo, *Geophys. Res. Lett.*, 34, L03 813, <https://doi.org/https://doi.org/10.1029/2006GL027648>, 2007.
- Chen, Y.-C., Christensen, M., Stephens, G. L., and Seinfeld, J. H.: Satellite-based estimate of global aerosol–cloud radiative forcing by marine warm clouds, *Nature Geosci.*, 7, 643–646, <https://doi.org/10.1038/ngeo2214>, 2014.
- Chen, Y.-S., Zhang, J., Glassmeier, F., Hoffmann, F., Yamaguchi, T., Zhou, X., and Feingold, G.: Diurnal evolution of non-precipitating stratocumuli in an LES ensemble, *EGUsphere*, 2024, 1–xx, 2024.
- Christensen, M. W., Ma, P.-L., Wu, P., Varble, A. C., Mülmenstädt, J., and Fast, J. D.: Evaluation of aerosol–cloud interactions in E3SM using a Lagrangian framework, *Atmos. Chem. Phys.*, 23, 2789–2812, <https://doi.org/10.5194/acp-23-2789-2023>, 2023.



- Chun, J.-Y., Wood, R., Blossey, P., and Doherty, S. J.: Microphysical, macrophysical, and radiative responses of subtropical marine clouds to aerosol injections, *Atmos. Chem. Phys.*, 23, 1345–1368, <https://doi.org/10.5194/acp-23-1345-2023>, 2023.
- Clough, S. A., Shephard, M. W., Mlawer, E. J., Delamere, J. S., Iacono, M. J., Cady-Pereira, K., Boukabara, S., and Brown, P. D.: Atmospheric radiative transfer modeling: A summary of the AER codes, *J. Quant. Spectrosc. Radiat. Transfer*, 91, 233–244, <https://doi.org/10.1016/j.jqsrt.2004.05.058>, 2005.
- Dagan, G., Yehekel, N., and Williams, A. I. L.: Radiative forcing from aerosol–cloud interactions enhanced by large-scale circulation adjustments, *Nat. Commun.*, 16, 1092–1098, <https://doi.org/10.1038/s41561-023-01319-8>, 2023.
- Diamond, M. S., Director, H. M., Eastman, R., Possner, A., and Wood, R.: Substantial Cloud Brightening From Shipping in Subtropical Low Clouds, *AGU Advances*, 1, e2019AV000 111, <https://doi.org/https://doi.org/10.1029/2019AV000111>, 2020.
- Feingold, G., Walko, R., Stevens, B., and Cotton, W.: Simulations of marine stratocumulus using a new microphysical parameterization scheme, *Atmos. Res.*, 47–48, 505–528, [https://doi.org/10.1016/S0169-8095\(98\)00058-1](https://doi.org/10.1016/S0169-8095(98)00058-1), 1998.
- Feingold, G., Eberhard, W. L., Veron, D. E., and Previdi, M.: First measurements of the Twomey indirect effect using ground-based remote sensors, *Geophys. Res. Lett.*, 30, <https://doi.org/10.1029/2002GL016633>, 2003.
- Feingold, G., McComiskey, A., Yamaguchi, T., Johnson, J. S., Carslaw, K. S., and Schmidt, K. S.: New approaches to quantifying aerosol influence on the cloud radiative effect, *Proc. Natl. Acad. Sci.*, 113, 5812–5819, <https://doi.org/10.1073/pnas.1514035112>, 2016.
- Feingold, G., Ghate, V. P., Russell, L. M., Blossey, P., Cantrell, W., Christensen, M. W., Diamond, M. S., Gettelman, A., Glassmeier, F., Grypsperdt, E., Haywood, J., Hoffmann, F., Kaul, C. M., Lebsock, M., McComiskey, A. C., McCoy, D. T., Ming, Y., Mülmenstädt, J., Possner, A., Prabhakaran, P., Quinn, P. K., Schmidt, K. S., Shaw, R. A., Singer, C. E., Sorooshian, A., Toll, V., Wan, J. S., Wood, R., Yang, F., Zhang, J., and Zheng, X.: Physical science research needed to evaluate the viability and risks of marine cloud brightening, *Sci. Adv.*, 10, eadi8594, <https://doi.org/10.1126/sciadv.adi8594>, 2024.
- Fons, E., Runge, J., Neubauer, D., and Lohmann, U.: Stratocumulus adjustments to aerosol perturbations disentangled with a causal approach, *npj Climate and Atmospheric Science*, 6, <https://doi.org/10.1038/s41612-023-00452-w>, 2023.
- Forster, P., Storelvmo, T., Armour, K., Collins, W., Dufresne, J.-L., Frame, D., Lunt, D. J., Mauritsen, T., Palmer, M. D., Watanabe, M., Wild, M., and Zhang, H.: The Earth’s Energy Budget, Climate Feedbacks, and Climate Sensitivity, in: *Climate Change 2021: The Physical Science Basis*, Contribution of Working Group I to the Sixth Assessment Report of the Intergovernmental Panel on Climate Change, edited by Masson-Delmotte, V., Zhai, P., Pirani, A., Connors, S. L., Péan, C., Berger, S., Caud, N., Chen, Y., Goldfarb, L., Gomis, M. I., Huang, M., Leitzell, K., Lonnoy, E., Matthews, J. B. R., Maycock, T. K., Waterfield, T., Yelekçi, O., Yu, R., and Zhou, B., pp. 923–1054, Cambridge University Press, Cambridge, United Kingdom and New York, NY, USA, 2021.
- Glassmeier, F., Hoffmann, F., Johnson, J. S., Yamaguchi, T., Carslaw, K. S., and Feingold, G.: An emulator approach to stratocumulus susceptibility, *Atmos. Chem. Phys.*, 19, 10 191–10 203, <https://doi.org/10.5194/acp-19-10191-2019>, 2019.
- Glassmeier, F., Hoffmann, F., Johnson, J. S., Yamaguchi, T., Carslaw, K. S., and Feingold, G.: Aerosol-cloud-climate cooling overestimated by ship-track data, *Science*, 371, 485–489, <https://doi.org/10.1126/science.abd3980>, 2021.
- Grypsperdt, E., Quaas, J., and Bellouin, N.: Constraining the aerosol influence on cloud fraction, *J. Geophys. Res.-Atmos.*, 121, 3566–3583, <https://doi.org/10.1002/2015JD023744>, 2016.
- Grypsperdt, E., Goren, T., Sourdeval, O., Quaas, J., Mülmenstädt, J., Dipu, S., Unglaub, C., Gettelman, A., and Christensen, M.: Constraining the aerosol influence on cloud liquid water path, *Atmos. Chem. Phys.*, 19, 5331–5347, <https://doi.org/10.5194/acp-19-5331-2019>, 2019.
- Grypsperdt, E., Goren, T., and Smith, T. W. P.: Observing the timescales of aerosol–cloud interactions in snapshot satellite images, *Atmos. Chem. Phys.*, 21, 6093–6109, <https://doi.org/10.5194/acp-21-6093-2021>, 2021.



- Gryspeerd, E., Glassmeier, F., Feingold, G., Hoffmann, F., and Murray-Watson, R. J.: Observing short-timescale cloud development to constrain aerosol–cloud interactions, *Atmos. Chem. Phys.*, 22, 11 727–11 738, <https://doi.org/10.5194/acp-22-11727-2022>, 2022.
- Hammersley, J. M. and Handscomb, D. C.: *Monte Carlo Methods*, Springer Dordrecht, Netherlands, 1964.
- 495 Hersbach, H., Bell, B., Berrisford, P., Hirahara, S., Horányi, A., Muñoz-Sabater, J., Nicolas, J., Peubey, C., Radu, R., Schepers, D., Simmons, A., Soci, C., Abdalla, S., Abellan, X., Balsamo, G., Bechtold, P., Biavati, G., Bidlot, J., Bonavita, M., De Chiara, G., Dahlgren, P., Dee, D., Diamantakis, M., Dragani, R., Flemming, J., Forbes, R., Fuentes, M., Geer, A., Haimberger, L., Healy, S., Hogan, R. J., Hólm, E., Janisková, M., Keeley, S., Laloyaux, P., Lopez, P., Lupu, C., Radnoti, G., de Rosnay, P., Rozum, I., Vamborg, F., Villaume, S., and Thépaut, J.-N.: The ERA5 global reanalysis, *Q. J. Roy. Meteor. Soc.*, 146, 1999–2049, <https://doi.org/10.1002/qj.3803>, 2020.
- 500 Hoffmann, F., Glassmeier, F., Yamaguchi, T., and Feingold, G.: Liquid Water Path Steady States in Stratocumulus: Insights from Process-Level Emulation and Mixed-Layer Theory, *J. Atmos. Sci.*, 77, 2203–2215, <https://doi.org/10.1175/JAS-D-19-0241.1>, 2020.
- Hoffmann, F., Glassmeier, F., Yamaguchi, T., and Feingold, G.: On the Roles of Precipitation and Entrainment in Stratocumulus Transitions between Mesoscale States, *J. Atmos. Sci.*, 80, 2791–2803, <https://doi.org/10.1175/JAS-D-22-0268.1>, 2023.
- Kazil, J., Wang, H., Feingold, G., Clarke, A. D., Snider, J. R., and Bandy, A. R.: Modeling chemical and aerosol processes in the transition from closed to open cells during VOCALS-REx, *Atmos. Chem. Phys.*, 11, 7491–7514, <https://doi.org/10.5194/acp-11-7491-2011>, 2011.
- 505 Kazil, J., Yamaguchi, T., and Feingold, G.: Mesoscale organization, entrainment, and the properties of a closed-cell stratocumulus cloud, *J. Adv. Model. Earth Syst.*, 9, 2214–2229, <https://doi.org/10.1002/2017MS001072>, 2017.
- Khairoutdinov, M. F. and Randal, D. A.: Cloud Resolving Modeling of the ARM Summer 1997 IOP: Model Formulation Results Uncertainties and Sensitivities, *J. Atmos. Sci.*, 60, 607–625, [https://doi.org/10.1175/1520-0469\(2003\)060<0607:CRMOTA>2.0.CO;2](https://doi.org/10.1175/1520-0469(2003)060<0607:CRMOTA>2.0.CO;2), 2003.
- 510 Latham, J. and Smith, M. H.: Effect on global warming of wind-dependent aerosol generation at the ocean surface, *Nature*, 347, 372–373, <https://doi.org/10.1038/347372a0>, 1990.
- Latham, J., Bower, K., Choullarton, T., Coe, H., Connolly, P., Cooper, G., Craft, T., Foster, J., Gadian, A., Galbraith, L., Iacovides, H., Johnston, D., Launder, B., Leslie, B., Meyer, J., Neukermans, A., Ormond, B., Parkes, B., Rasch, P., Rush, J., Salter, S., Stevenson, T., Wang, H., Wang, Q., and Wood, R.: Marine cloud brightening, *Philos. trans., Math. phys. eng. sci.*, 370, 4217–4262, <https://doi.org/10.1098/rsta.2012.0086>, 2012.
- 515 McComiskey, A. and Feingold, G.: The scale problem in quantifying aerosol indirect effects, *Atmos. Chem. Phys.*, 12, 1031–1049, <https://doi.org/10.5194/acp-12-1031-2012>, 2012.
- Morris, M. D. and Mitchell, T. J.: Exploratory designs for computational experiments, *Journal of Statistical Planning and Inference*, 43, 381–402, [https://doi.org/10.1016/0378-3758\(94\)00035-T](https://doi.org/10.1016/0378-3758(94)00035-T), 1995.
- 520 Mülmenstädt, J., Gryspeerd, E., Dipu, S., Quaas, J., Ackerman, A. S., Fridlind, A. M., Tornow, F., Bauer, S. E., Gettelman, A., Ming, Y., Zheng, Y., Ma, P.-L., Wang, H., Zhang, K., Christensen, M. W., Varble, A. C., Leung, L. R., Liu, X., Neubauer, D., Partridge, D. G., Stier, P., and Takemura, T.: General circulation models simulate negative liquid water path–droplet number correlations, but anthropogenic aerosols still increase simulated liquid water path, *EGUsphere*, 2024, 1–29, <https://doi.org/10.5194/egusphere-2024-4>, 2024.
- Mülmenstädt, J. and Feingold, G.: The Radiative Forcing of Aerosol–Cloud Interactions in Liquid Clouds: Wrestling and Embracing Uncertainty, *Curr. Clim. Change Rep.*, 4, 23–40, <https://doi.org/10.1007/s40641-018-0089-y>, 2018.
- 525 National Academies of Sciences, Engineering, and Medicine (NASEM) report: Reflecting Sunlight: Recommendations for Solar Geoengineering Research and Research Governance, The National Academies Press, Washington, DC, USA, <https://doi.org/10.17226/25762>, 2021.



- 530 Petters, J. L., Harrington, J. Y., and Clothiaux, E. E.: Radiative–Dynamical Feedbacks in Low Liquid Water Path Stratiform Clouds, *J. Atmos. Sci.*, 69, 1498–1512, <https://doi.org/10.1175/JAS-D-11-0169.1>, 2012.
- Platnick, S. and Twomey, S.: Determining the susceptibility of cloud albedo to changes in droplet concentration with the advanced very high resolution radiometer, *J. Appl. Meteorol.*, 33, 334–347, [https://doi.org/10.1175/1520-0450\(1994\)033<0334:DTSOCA>2.0.CO;2](https://doi.org/10.1175/1520-0450(1994)033<0334:DTSOCA>2.0.CO;2), 1994.
- Possner, A., Eastman, R., Bender, F., and Glassmeier, F.: Deconvolution of boundary layer depth and aerosol constraints on cloud water path in subtropical stratocumulus decks, *Atmos. Chem. Phys.*, 20, 3609–3621, <https://doi.org/10.5194/acp-20-3609-2020>, 2020.
- 535 Prabhakaran, P., Hoffmann, F., and Feingold, G.: Evaluation of Pulse Aerosol Forcing on Marine Stratocumulus Clouds in the Context of Marine Cloud Brightening, *J. Atmos. Sci.*, 80, 1585–1604, <https://doi.org/10.1175/JAS-D-22-0207.1>, 2023.
- Prabhakaran, P., Hoffmann, F., and Feingold, G.: Effects of intermittent aerosol forcing on the stratocumulus-to-cumulus transition, *Atmos. Chem. Phys.*, 24, 1919–1937, <https://doi.org/10.5194/acp-24-1919-2024>, 2024.
- Qiu, S., Zheng, X., Painemal, D., Terai, C. R., and Zhou, X.: Daytime variation in the aerosol indirect effect for warm marine boundary layer clouds in the eastern North Atlantic, *Atmos. Chem. Phys.*, 24, 2913–2935, <https://doi.org/10.5194/acp-24-2913-2024>, 2024.
- 540 Sandu, I., Brenguier, J.-L., Geoffroy, O., Thouron, O., and Masson, V.: Aerosol Impacts on the Diurnal Cycle of Marine Stratocumulus, *J. Atmos. Sci.*, 65, 2705–2718, <https://doi.org/10.1175/2008JAS2451.1>, 2008.
- Smalley, K. M., Lebsock, M. D., and Eastman, R.: Diurnal Patterns in the Observed Cloud Liquid Water Path Response to Droplet Number Perturbations, *Geophys. Res. Lett.*, 51, e2023GL107323, <https://doi.org/https://doi.org/10.1029/2023GL107323>, 2024.
- 545 Stephens, G. L., Li, J., Wild, M., Clayson, C. A., Loeb, N., Kato, S., L’Ecuyer, T., Stackhouse, P. W., Lebsock, M., and Andrews, T.: An update on Earth’s energy balance in light of the latest global observations, *Nature Geosci.*, 5, 691–696, <https://doi.org/10.1038/ngeo1580>, 2012.
- Stevens, B. and Feingold, G.: Untangling aerosol effects on clouds and precipitation in a buffered system, *Nature*, 461, 607–613, <https://doi.org/10.1038/nature08281>, 2009.
- 550 Stier, P.: Limitations of passive remote sensing to constrain global cloud condensation nuclei, *Atmos. Chem. Phys.*, 16, 6595–6607, <https://doi.org/10.5194/acp-16-6595-2016>, 2016.
- Toll, V., Christensen, M., Quaas, J., and Bellouin, N.: Weak average liquid-cloud-water response to anthropogenic aerosols, *Nature*, 572, 51–55, <https://doi.org/10.1038/s41586-019-1423-9>, 2019.
- Twomey, S.: Pollution and the planetary albedo, *Atmospheric Environment*, 8, 1251–1256, [https://doi.org/10.1016/0004-6981\(74\)90004-3](https://doi.org/10.1016/0004-6981(74)90004-3), 555 1974.
- Twomey, S.: The Influence of Pollution on the Shortwave Albedo of Clouds, *J. Atmos. Sci.*, 34, 1149–1152, [https://doi.org/10.1175/1520-0469\(1977\)034<1149:TIOPOT>2.0.CO;2](https://doi.org/10.1175/1520-0469(1977)034<1149:TIOPOT>2.0.CO;2), 1977.
- Wang, H. and Feingold, G.: Modeling Mesoscale Cellular Structures and Drizzle in Marine Stratocumulus Part I: Impact of Drizzle on the Formation and Evolution of Open Cells, *J. Atmos. Sci.*, 66, 3237–3256, <https://doi.org/10.1175/2009JAS3022.1>, 2009.
- 560 Wang, S., Wang, Q., and Feingold, G.: Turbulence, Condensation, and Liquid Water Transport in Numerically Simulated Nonprecipitating Stratocumulus Clouds, *J. Atmos. Sci.*, 60, 262–278, [https://doi.org/10.1175/1520-0469\(2003\)060<0262:TCALWT>2.0.CO;2](https://doi.org/10.1175/1520-0469(2003)060<0262:TCALWT>2.0.CO;2), 2003.
- Wood, R.: Stratocumulus Clouds, *Mon. Wea. Rev.*, 140, 2373–2423, <https://doi.org/10.1175/MWR-D-11-00121.1>, 2012.
- Wood, R.: Assessing the potential efficacy of marine cloud brightening for cooling Earth using a simple heuristic model, *Atmos. Chem. Phys.*, 21, 14 507–14 533, <https://doi.org/10.5194/acp-21-14507-2021>, 2021.
- 565 Xue, H. and Feingold, G.: Large-Eddy Simulations of Trade Wind Cumuli: Investigation of Aerosol Indirect Effects, *J. Atmos. Sci.*, 63, 1605–1622, <https://doi.org/10.1175/JAS3706.1>, 2006.



- Yamaguchi, T., Feingold, G., and Kazil, J.: Stratocumulus to Cumulus Transition by Drizzle, *J. Adv. Model. Earth Syst.*, 9, 2333–2349, <https://doi.org/10.1002/2017MS001104>, 2017.
- 570 Yamaguchi, T., Feingold, G., and Kazil, J.: Aerosol-Cloud Interactions in Trade Wind Cumulus Clouds and the Role of Vertical Wind Shear, *J. Geophys. Res.-Atmos.*, 124, 12 244–12 261, <https://doi.org/https://doi.org/10.1029/2019JD031073>, 2019.
- Zhang, J. and Feingold, G.: Distinct regional meteorological influences on low-cloud albedo susceptibility over global marine stratocumulus regions, *Atmos. Chem. Phys.*, 23, 1073–1090, <https://doi.org/10.5194/acp-23-1073-2023>, 2023.
- Zhang, J., Zhou, X., Goren, T., and Feingold, G.: Albedo susceptibility of northeastern Pacific stratocumulus: the role of covarying meteorological conditions, *Atmos. Chem. Phys.*, 22, 861–880, <https://doi.org/10.5194/acp-22-861-2022>, 2022.
- 575 Zhou, X. and Feingold, G.: Impacts of Mesoscale Cloud Organization on Aerosol-Induced Cloud Water Adjustment and Cloud Brightness, *Geophys. Res. Lett.*, 50, e2023GL103 417, <https://doi.org/https://doi.org/10.1029/2023GL103417>, 2023.
- Zhou, X., Zhang, J., and Feingold, G.: On the Importance of Sea Surface Temperature for Aerosol-Induced Brightening of Marine Clouds and Implications for Cloud Feedback in a Future Warmer Climate, *Geophys. Res. Lett.*, 48, e2021GL095 896, <https://doi.org/10.1029/2021GL095896>, 2021.

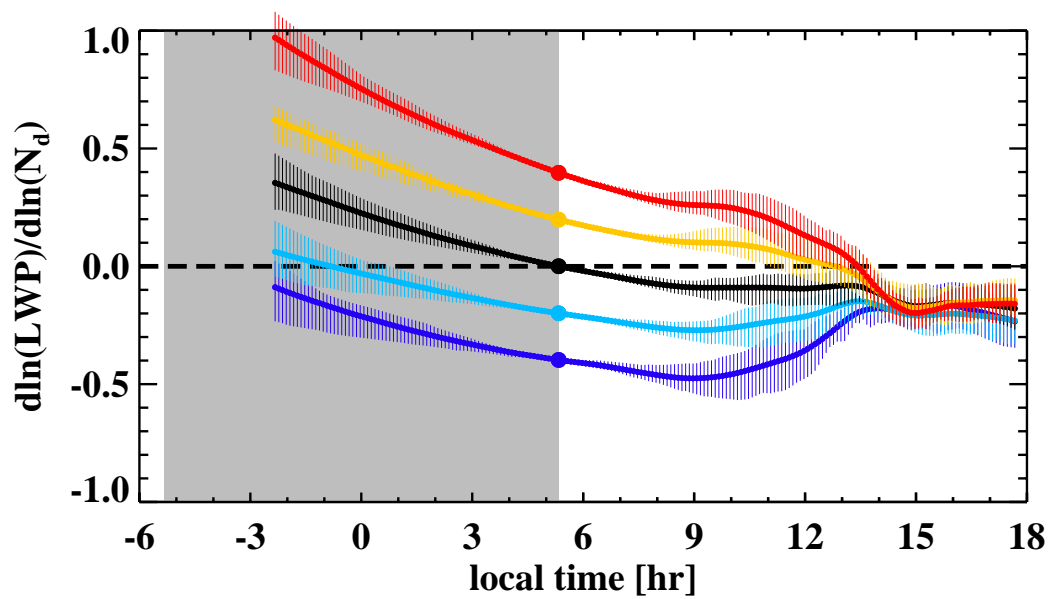


Figure 1. Diurnal cycle of N_d -LWP regression slope ($d\ln(\text{LWP})/d\ln(N_d)$). Solid lines indicate mean values of the 50 25-member cMC subsampling for individual groups, which are separated by colors representing different $d\ln(\text{LWP})/d\ln(N_d)$ values at sunrise (large dots): 0.4 (red), 0.2 (yellow), 0.0 (black), -0.2 (cyan), and -0.4 (blue). Vertical bars indicate interquartile ranges for each group. A 1-hour running mean is applied. Gray shading indicates nighttime hours.

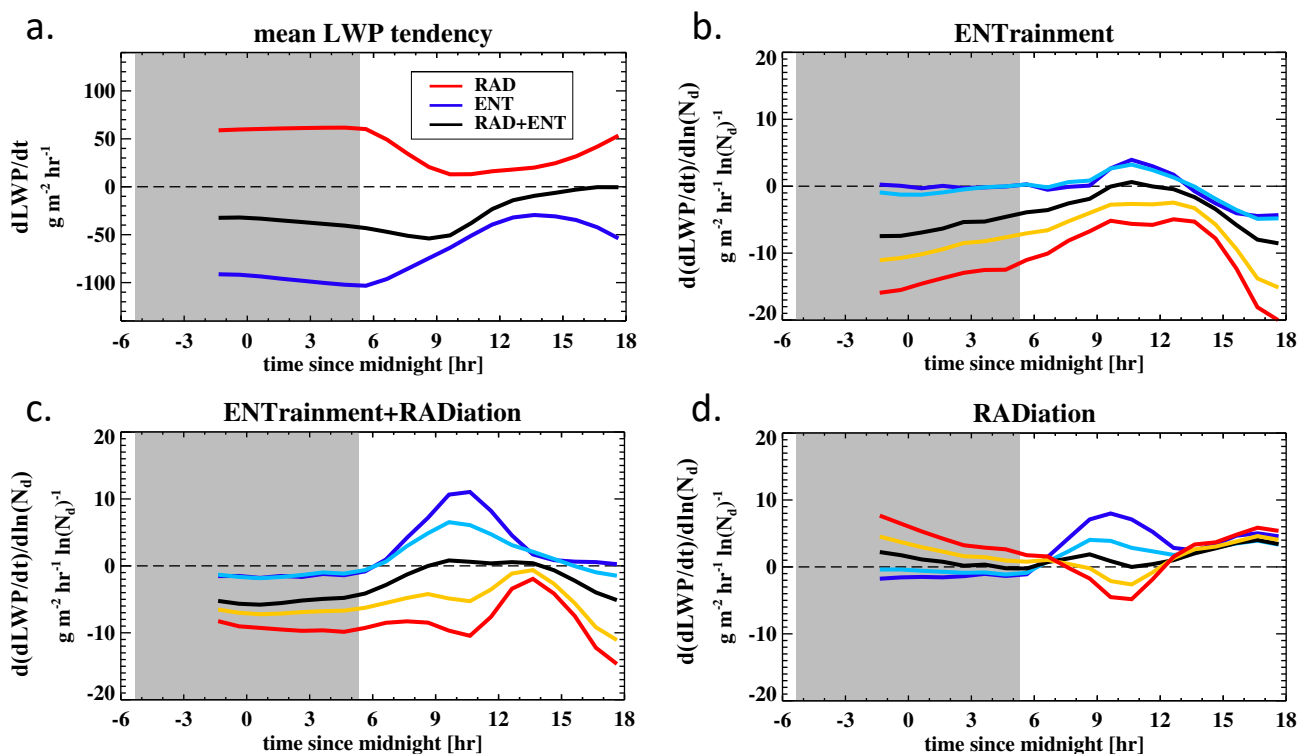


Figure 2. Diurnal cycle of (a) mean LWP tendencies attributed to radiation (RAD), entrainment (ENT) and the sum of RAD and ENT (RAD+ENT), and (b-d) their sensitivity to N_d . Mean sensitivity evolutions are shown for the five groups with different prescribed N_d -LWP relationships ($d\ln(LWP)/d\ln(N_d)$) at sunrise, whose evolutions in $d\ln(LWP)/d\ln(N_d)$ are shown in Fig. 1. A 1-hour running mean is applied. Gray shading indicates nighttime hours.

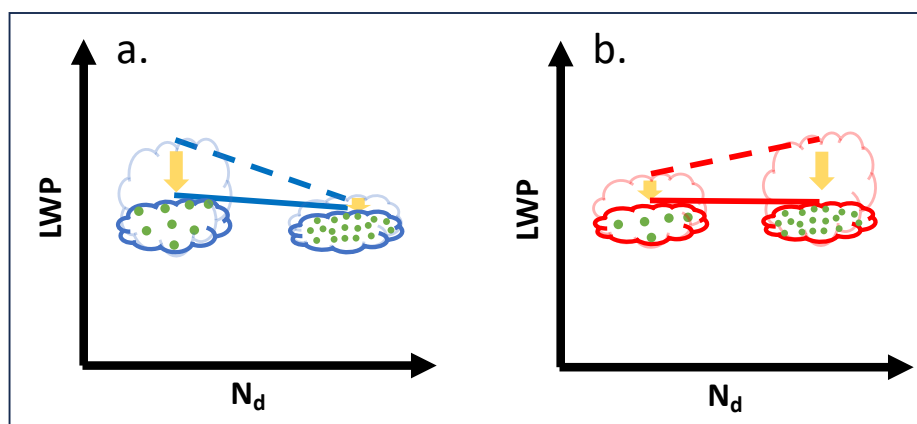


Figure 3. A schematic illustrating the hypothesis for the cause of the buffered daytime evolution in N_d -LWP relationship – that is thicker clouds thin faster whereas thinner clouds thin slower, resulting in flattened slopes (solid lines) regardless of the initial slope at sunrise (dashed lines). Blue (red) “clouds” represent the blue (red) group in Fig. 1.

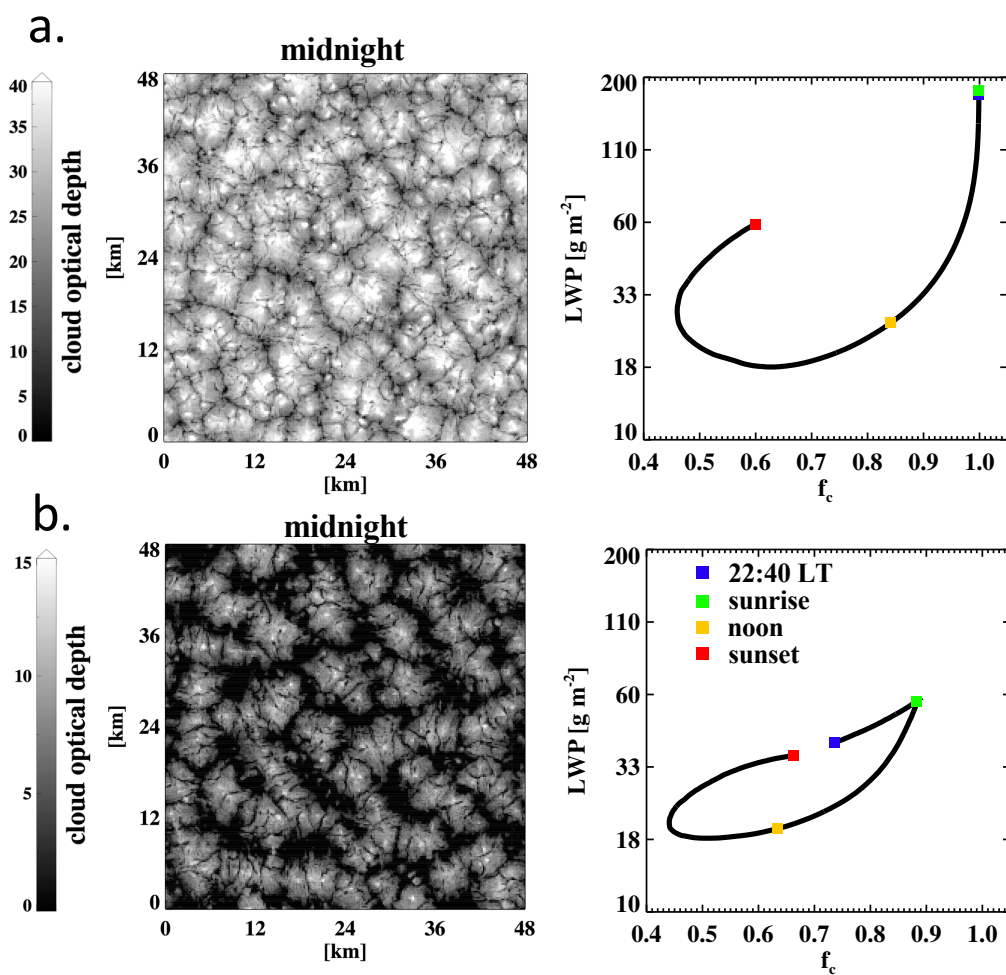


Figure 4. (left column) Example 2D snapshots of cloud optical depth at local midnight (hour 6 of the simulation time) and (right column) mean diurnal cycle of LWP and cloud fraction (f_c) of the simulated 'closed' and (non-precipitating) 'open' cell Sc. Sunrise, sunset, noon, as well as 22:40 LT (end of spin-up) are indicated on the diurnal cycle.

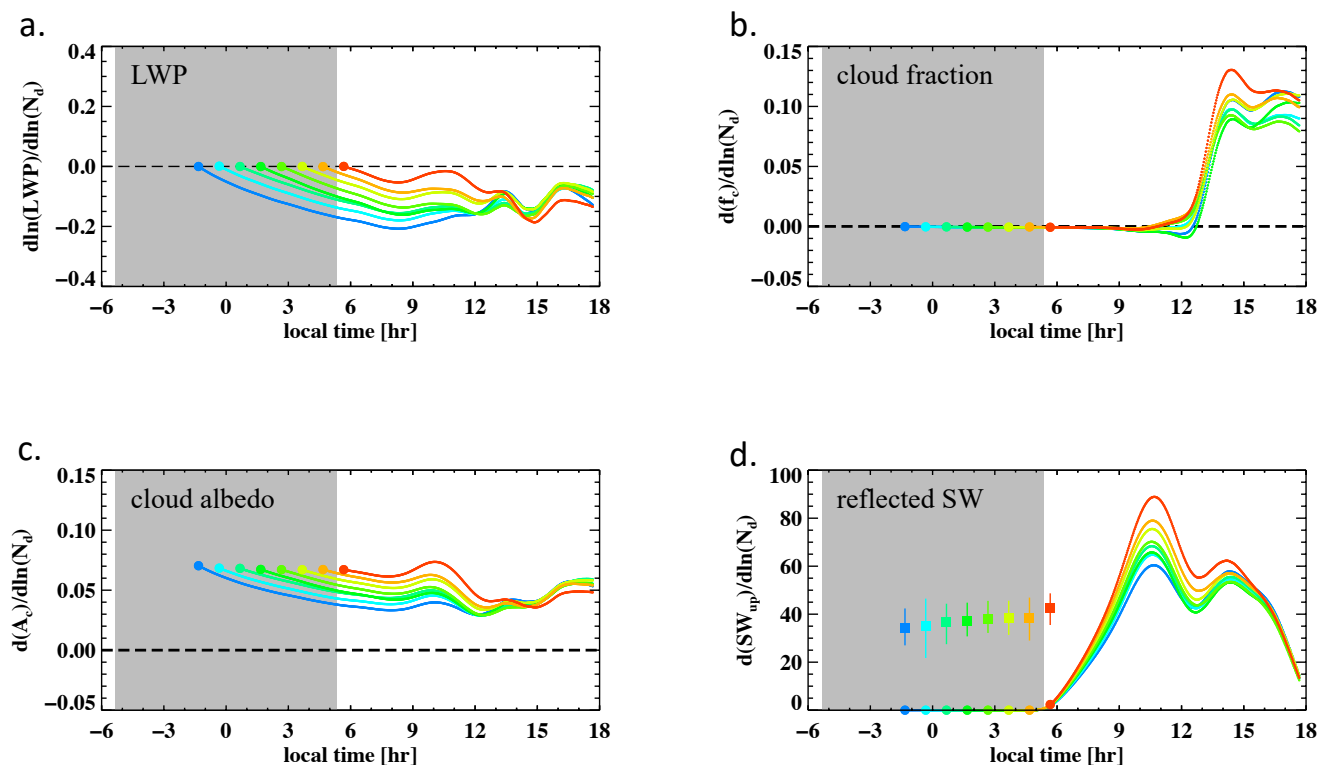


Figure 5. Diurnal cycle of (a) $\frac{d\ln(\text{LWP})}{d\ln(N_d)}$, (b) $\frac{df_c}{d\ln(N_d)}$, (c) $\frac{dA_c}{d\ln(N_d)}$, and (d) $\frac{d\text{SW}_{\text{up}}}{d\ln(N_d)}$. Colors separate groups mimicking “aerosol perturbation” at different times when $\frac{d\ln(\text{LWP})}{d\ln(N_d)}$ and $\frac{df_c}{d\ln(N_d)}$ are set to ~ 0 . Mean values averaged over 50 repeated cMC samplings of each group are shown. Relationships between N_d and diurnally integrated reflected SW (i.e., $d(\int \text{SW}_{\text{up}} dt)/d\ln(N_d)$) for different perturbation times are shown as filled squares with interquartile ranges using the same color scheme. A 1-hour running mean is applied. Gray shading indicates nighttime hours.

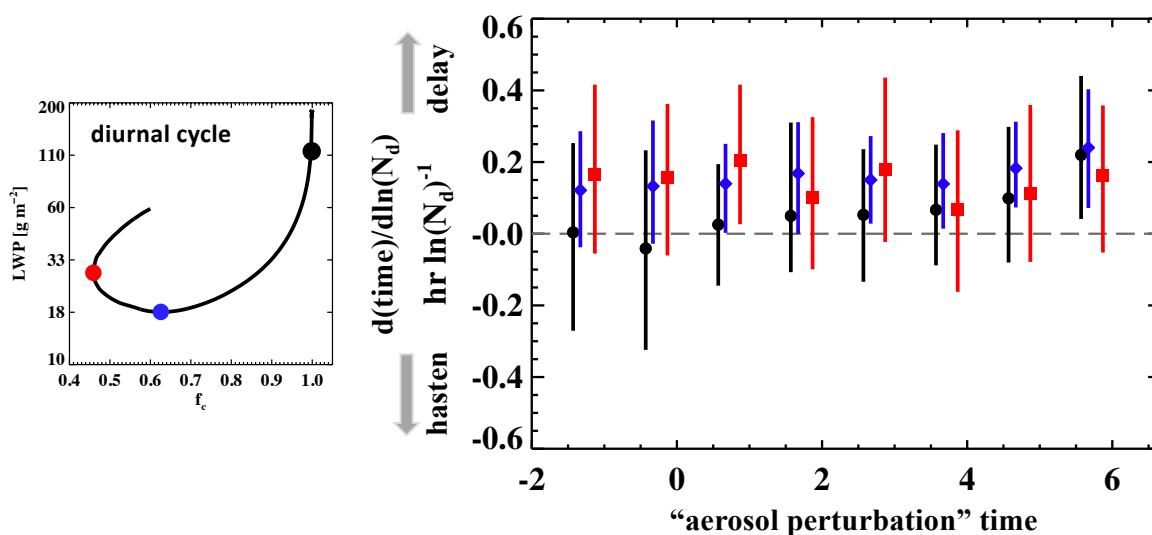


Figure 6. Relationships between N_d and overcast closed-cell Sc diurnal cycle critical times, i.e., $d(\text{time}_{\text{critical}})/d\ln(N_d)$, which include the time when cloud breaks up ($f_c < 0.95$; black), reaches minimum-LWP (blue), and reaches minimum- f_c (red), for different “aerosol perturbation” times. Mean values and interquartile ranges are shown. The left-hand-side diagram is the same as that in Fig. 5a, for the illustration of critical times in the diurnal cycle.

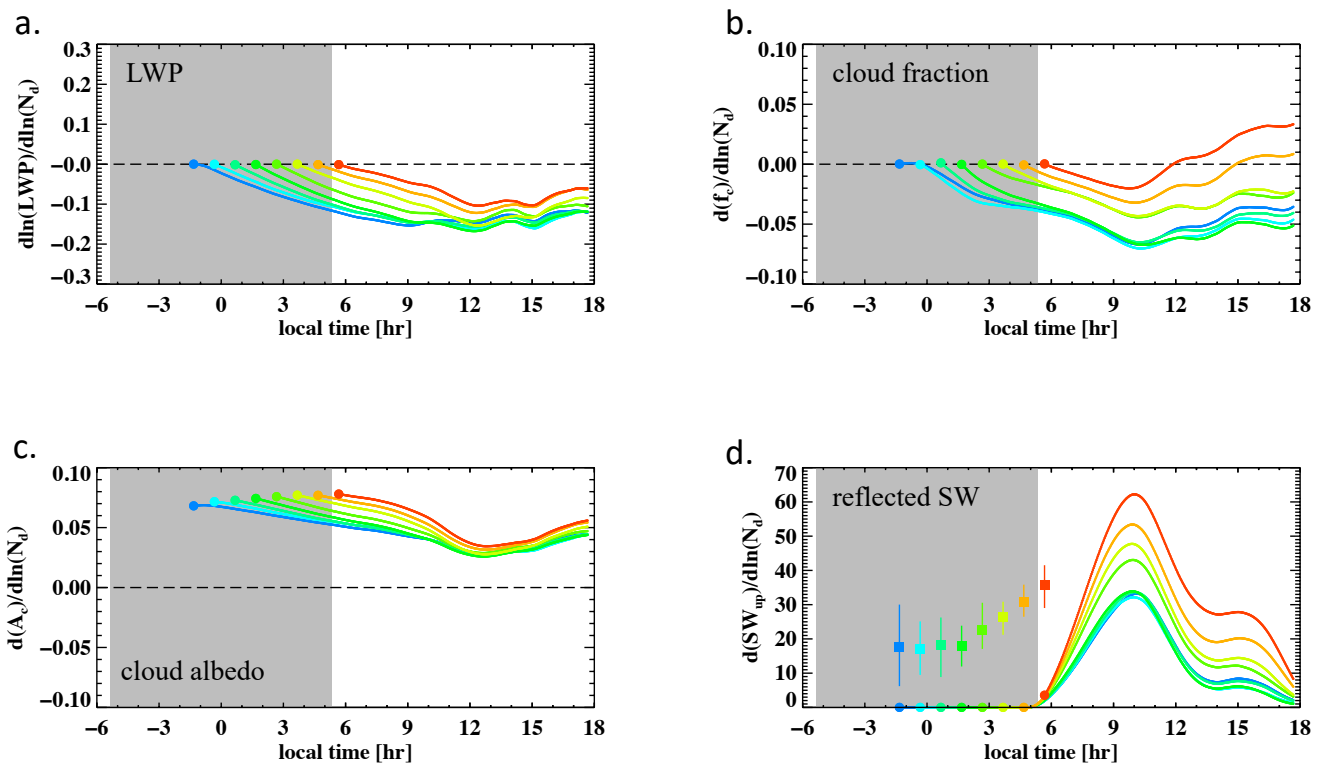


Figure 7. As in Fig. 5, but for the non-precipitating open-cell Sc class.

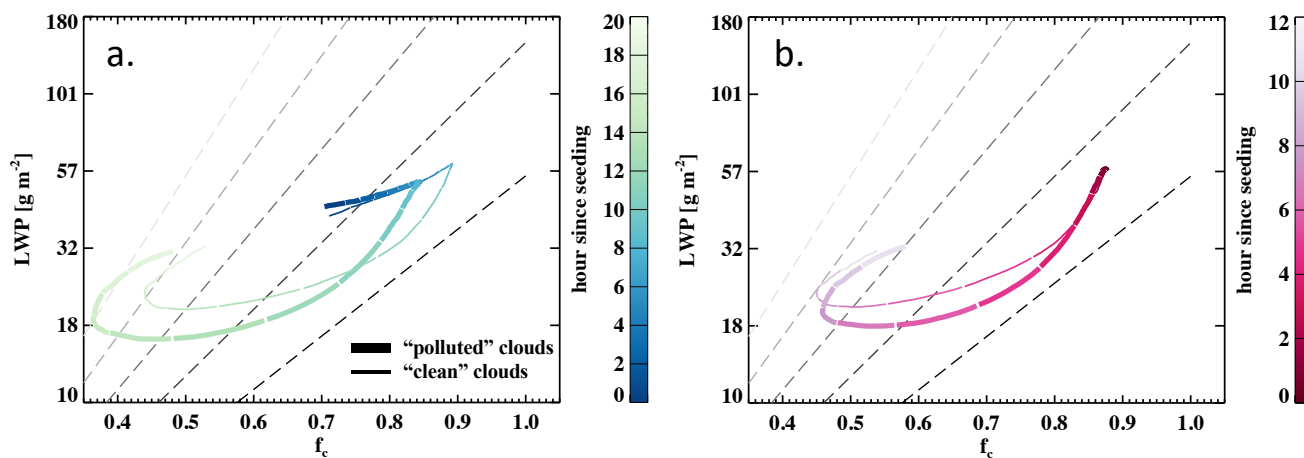


Figure 8. Diurnal cycle of cloud evolution in LWP– f_c space, for (a) the earliest and (b) the latest (at sunrise) “aerosol perturbation” groups. Thick lines represent the mean evolution of the highest 20% of the members in N_d (“polluted” clouds, high- N_d), whereas the thinner lines indicate the lowest 20% in N_d (“clean” clouds, low- N_d). Lines are colored and separated at every hour since the “aerosol perturbation”. Gray-scale dashed isolines in the background indicate a rough measure of cloud aspect ratio, approximated by the ratio of $\ln(\text{LWP})$ to f_c . Darker lines indicate more stratiform clouds and lighter lines indicate more cumuliform clouds.